J Mol Model (2003) 9:372–378
DOI 10.1007/s00894-003-0142-0

ORIGINAL PAPER

Artur Giełdoń · Rajmund Kaźmierkiewicz · Rafał Ślusarz · Marta Pasenkiewicz-Gierula · Jerzy Ciarkowski

Molecular dynamics study of 4-OH-phenylacetyl-*D*-Y(Me)FQNRPR-NH_2 selectivity to V1a receptor

Received: 5 December 2002 / Accepted: 16 May 2003 / Published online: 7 October 2003

Abstract G protein-coupled receptors relay diverse extracellular signals into cells via a common mechanism, involving activation of cytosol G proteins. The mechanism underlies the actions of ~50% of all drugs. In this work, we focus on simulating three protein–ligand complexes of the neurohypophyseal hormone analog 4-OH-phenylacetyl-*D*-Y(Me)FQNRPR-NH_2 (**I**) with the human V1a, V2 and oxytocin receptors. The peptide **I** is a potent selective V1a receptor antagonist. To obtain relaxed models of the complexes, the following techniques were used: docking of **I** into the vasopressin V1a, V2 and oxytocin receptor models, optimization of the geometry of the resulting complexes and molecular dynamics in a fully hydrated 1-palmitoyl-2-oleoyl-*sn*-glycero-3-phosphatidylcholine lipid bilayer. The results of the simulations allow us to draw some conclusions about the ligand selectivity to V1aR.

Keywords Amber · AutoDock · GPCR receptor–bioligand interaction · Molecular dynamics · OT/VP receptors · Antagonist · Linear peptide

Introduction

The neurohypophyseal hormone arginine vasopressin (CYFQNCPRG-NH_2, AVP) is a nonapeptide-amide (partly cyclic via the C1–C6 disulfide), whose actions are mediated by specific G-protein coupled receptors (GPCRs), viz. V1a vascular, V2 renal and V1b pituitary receptors (V1aR, V2R and V1bR, respectively). AVP is involved in a number of physiological functions, including the regulation of body-fluid osmolality, blood volume, vascular tone and blood pressure. [1, 2] A related hormone oxytocin (OT=[Ile3,Leu8]AVP) regulates labor and lactation in mammalian females, via interactions with OT receptors (OTR). [2, 3] All four receptors belong to the Class A or rhodopsin-like GPCR family, with rhodopsin (RD) being its archetype member. [4, 5] The neurohypophyseal human receptors share a high degree (35–50%) of sequence identity, [6, 7] see Table 1. Yet, V1aR, V1bR and OTR are selectively coupled to $G_{q/11}$ proteins, [8] mediating the activation of phospholipase Cβ, controlling the breakdown of phosphoinositide lipids. The V2 receptor, on the other hand, activates the G_s protein, [8] which results in the activation of adenylyl cyclase. This is to an extent reflected in the sequence similarities, higher among the V1aR, V1bR and OTR than between any of them and V2R, see Table 1, even more profound in the intracellular loops 2 and 3, whose sequences are very well conserved among V1aR, V1bR and OTR (50 to 78% identity) but diverge with the V2R subtype (23 to 30% identity with the former ones). [7] Interestingly, in accord with this property, Liu and Wess have recently provided evidence that IL3 of V2R plays a decisive role in the G_s protein–adenylyl cyclase coupling, while IL2 of V1aR, V1bR and OTR play a decisive role in the coupling of the $G_{q/11}$ protein to phospholipase C. [9] In contrast to the differences on the intracellular side, the extracellular sides of the four receptors do not differ significantly among themselves. In fact the extracellular loop 2 (EL2) and the C-terminal part of EL3 belong,

A. Giełdoń (✉) · R. Kaźmierkiewicz · R. Ślusarz · J. Ciarkowski
Faculty of Chemistry,
University of Gdańsk,
Sobieskiego 18, 80-952 Gdańsk, Poland
e-mail: lukasz@chem.univ.gda.pl

M. Pasenkiewicz-Gierula
Institute of Molecular Biology,
Jagiellonian University,
Gronostajowa 7, 30-387 Kraków, Poland

Table 1 Identity matrix for human V2R, V1aR, V1bR and OTR as given in [6, 7], extended to include RD, using Clustal W-based multiple sequence alignment [14]

	V2R	V1aR	V1bR	OT
V1aR	0.35			
V1bR	0.40	0.47		
OTR	0.40	0.44	0.48	
RD	0.14	0.14	[a]	0.17

[a] Not tested

together with the helices TM2, TM3 TM6 and TM7, to the most conserved parts among the four [6, 7] with identity reaching 87%. In this respect, it is reasonable to assume more or less common recognition and binding modes for both OT and VP in their host receptors, even if certain residues in equivalent positions diverge and some of them, i.e. D103 in EL1 of V2R, F and Y in equivalent positions of OTR and V1aR/V1bR, respectively, are suggested to be responsible for hormone selectivity. [10, 11] This ambiguity warrants more involved studies on receptor–ligand interactions to explain the selectivity of both agonists and antagonists to V1aR, V2T and OTR. Perhaps the most notable feature on the extracellular side, common to a majority of GPCRs, is a putative disulphide bond, keeping EL1 and EL2 together, made of two invariant cysteines from the EL1/TM3 boundary and the middle of EL2. [5]

Table 1 also includes, for comparison, the data on similarities of V2R, V1aR and OTR to RD. The relatively small values in the last row are considerably higher for the 7TM domain alone and average between 0.32 (for helices TM1 and TM4) to 0.49 (for TM6).

4-OH-Phaa-*D*-Y(Me)-FQNRPR-NH_2 (desG9-[OH-Phaa1,*D*-(Me)Y2,R6]AVP (**I**), where OH-Phaa=4-OH-phenylacetyl, is a potent V1aR linear peptide antagonist. [12] Current molecular modeling tools potentially enable reasonably detailed knowledge about receptor structure and ligand–receptor interactions and thus may be of substantial help in rational drug design. [13] In this work, we present the results of molecular docking, followed by 1-ns molecular dynamics (MD), of **I** in V1aR, V2R and OTR, leading to structural arguments for its selectivity to V1aR.

Methods

The recent structure of dark rhodopsin (RD) at 2.8-Å resolution [4] was used as a template to build antagonist-bound three-dimensional V1aR, V2R and OTR models. Standard techniques, including protein multiple sequence alignment, [14, 15] followed by homology modeling and loop-building (*loop search*), as implemented in SYBYL, [16] were used. The approach used by SYBYL *loop search* relies on finding fragments in the loop database of a fragment having a proper sequence length whose anchor regions have a good geometric fit to the anchor regions of the modeled protein. The procedure typically returns several candidate loops that satisfy the geometrical and homological requirements. Having accordingly replaced and/or stitched missing (IL3 and IL4) fragments in the original RD, the conserved disulfide bridge between TM3 and EL2 was added. The conserved Cys–Cys pair terminating helix 8 was palmitoylated, to mimic IL4. [17,18] The palmitoylcystein (PAL) residues, absent in the AMBER database, were parameterized by dividing them into two similar-length segments, with atomic point-charge calculations for two conformations per segment at the ab initio RHF/6–31G* level using the GAMESS program, [19] and subsequent conformational-averaging of the charges over the whole PAL group using the RESP procedure [20] as recommended in the AMBER manual. [21] For more details see [22, 23]. The non-standard residues OH–Phaa and D-Tyr(Me) in the ligand were constructed using the crystallographic database CSDS [24] and parameterized as above. The starting V1aR, V2R and OTR models were minimized (5,000 steepest descent steps) using the AMBER 5.0 [21] force field. The ligand was docked into the receptors using the AutoDock version 3.0 program [25] with the implemented genetic algorithm. About 80 complexes were sampled for each ligand–receptor system, of which about 30 of the lowest-energy ones were relaxed using a constrained simulated annealing (CSA) [26] protocol in vacuo, as implemented in AMBER 5.0, [21] with frozen transmembrane C^{α} and PAL atoms, to keep the receptor shape. The two lowest-energy receptor–ligand complexes were selected from each set and immersed into the fully hydrated ~10-ns equilibrated 1-palmitoyl-2-oleoyl-*sn*-glycero-3-phosphatidylcholine (POPC) lipid bilayer, [22, 23, 27] using a home-made algorithm. Each of the six resultant systems consisted of 120 lipid molecules, the protein of ca. 340–350 amino acid residues, 16, 14 and 15 Cl^- counter-ions for V1aR, V2R and OTR, respectively, and ~7,300 water molecules; ~32,000 atoms total in the periodic rectangular box of 75 Å×65 Å×93 Å approximate size. After a routine energy minimization, and 40 ps relaxation with frozen C^{α} atoms in the receptor, the systems were submitted to periodic boundary MD with 12 Å single cut-off and constant pressure, as implemented in AMBER 5.0. [21] In all MD simulations, the time step was 1 fs and all atoms were free to move. The productive simulations were 1 ns long and they were performed on an INTEL XEON 700 MHz 128-processor cluster in the Academic Computer Center in Gdańsk (CI TASK). The receptor–ligand and/or interhelical interaction energy was measured using the program ANAL within the AMBER package. Due to the nature of force-field parameterized methods, it is useful to make comparisons between conformers of *the same system* but not for comparisons (of affinities etc.) *between different receptor–ligand systems*; hence we omit any quantitative reference to energy terms in this work.

Results and discussion

In this work we intend first to identify conformational changes in the receptor–ligand complexes that accompany 1-ns MD and, secondly, to recognize the receptor residues responsible for interactions with the ligand. As our starting models relied on RD as a common template, the initial V2R, V1aR and OTR architectures were very similar. In particular, the conserved residues occupied equivalent sites in the three receptors and built up similar sets of mutual and extended interactions, summarized in Table 2. We calculated the distances between all possible pairs of atoms for any pair of residues in the protein–ligand complex. Two residues were considered interacting if the contact distance between any two atoms from these pairs was less than 4.5 Å.

Using the common conserved residues as reference pointers, we tried to define conformational changes in the receptors during the MD. Apart from the residue–residue contact distances as defined above, the sums of energy terms corresponding to the interactions between helices were measured (see Methods); these values serve only as a guide and are not given, as they have no physical meaning. The residues interacting with each other before and after molecular dynamics are marked gray in Table 3. Thus, in the 1-ns timescale conserved stable interactions in the V1a receptor are retained between the following transmembrane helix pairs: strong (involving three or more residue pairs) TM1–TM2 and TM3–TM4; medium (via two residue pairs) TM1–TM7, TM2–TM3, TM2–TM4, TM3–TM5 and TM6–TM7; weak (via one residue pair) TM2–TM7, TM3–TM6 and TM5–TM6, see Table 2. TM5 loses almost all its interactions with other helices

Table 2 Conservative residues for the neurophypophyseal and Class A (bold) GPCR family, in both starting structures at distances potentially enabling interactions with each other. The Class A consensus numbering [30] is also given for reference. The residues interacting with each other before and after molecular dynamics are marked gray. A pair of residues is considered interacting if the distance between any two atoms in this pair is less than 4.5 Å

Helix	[a]	V2R	V1aR	OTR		Helix	[a]	V2R	V1aR	OTR
TM1	1.39	L44	L58	L46	–	TM2	2.58	V93	V105	V93
TM1	1.42	V47	T61	I49	–	TM7	7.47	C319	C342	C323
TM1	1.43	F48	F62	L50	–	TM2	2.54	A89	A101	A89
TM1	1.43	F48	F62	L50	–	TM2	2.58	V93	V105	V93
TM1	**1.46**	**V51**	**A65**	**A53**	–	TM7	7.47	C319	C342	C323
TM1	**1.50**	**N55**	**N69**	**N57**	–	TM2	2.47	C82	S94	S82
TM1	**1.53**	**V58**	**V72**	**V60**	–	TM7	**7.50**	**P322**	**P345**	**P326**
TM1	1.54	L59	L73	L61	–	TM2	2.44	G79	R91	K79
TM1	1.57	L62	L76	L64	–	TM2	2.40	H75	H87	F75
TM2	2.41	V76	L88	F76	–	TM4	4.46	V160	I171	V157
TM2	2.42	F77	F89	F77	–	TM4	4.46	V160	I171	V157
TM2	2.43	I78	I90	M78	–	TM7	**7.53**	**Y325**	**Y348**	**Y329**
TM2	**2.45**	**H80**	**H92**	**H80**	–	TM4	4.46	V160	I171	V157
TM2	**2.45**	**H80**	**H92**	**H80**	–	TM4	**4.50**	**W164**	**W175**	**W161**
TM2	**2.50**	**D85**	**D97**	**D85**	–	TM7	**7.46**	**S318**	**S341**	**S322**
TM2	**2.53**	**V88**	**V100**	**V88**	–	TM7	**7.46**	**S318**	**S341**	**S322**
TM2	**2.53**	**V88**	**V100**	**V88**	–	TM3	3.35	G122	G134	G122
TM2	2.56	F91	F103	F91	–	TM3	3.31	L118	L130	L118
TM2	2.57	Q92	Q104	Q92	–	TM3	3.27	A114	V126	L114
TM2	2.57	Q92	Q104	Q92	–	TM3	3.32	Q119	Q131	Q119
TM2	2.60	P95	P107	P95	–	TM3	3.28	V115	V127	V115
TM2	2.61	Q96	Q108	Q96	–	TM3	3.28	V115	V127	V115
TM2	2.64	W99	W111	W99	–	TM3	3.24	L111	L123	L111
TM2	2.64	W99	W111	W99	–	TM3	**3.25**	**C112**	**C124**	**C112**
TM3	3.26	R113	R125	R113	–	TM4	4.61	L175	Y186	V172
TM3	3.34	V121	F133	V121	–	TM4	4.54	L168	F179	L165
TM3	3.36	M123	M135	M123	–	TM6	**6.48**	**W284**	**W304**	**W288**
TM3	3.37	Y124	F136	F124	–	TM4	4.53	S167	S178	C164
TM3	3.37	Y124	F136	F124	–	TM5	5.46	V213	I224	V208
TM3	3.38	A125	A137	A125	–	TM4	4.53	S167	S178	C164
TM3	3.41	Y128	Y140	Y128	–	TM4	4.48	V162	A173	A159
TM3	3.41	Y128	Y140	Y128	–	TM4	4.49	A163	A174	T160
TM3	3.42	M129	M141	L129	–	TM4	4.49	A163	A174	T160
TM3	**3.43**	**I130**	**L142**	**L130**	–	TM5	5.54	I221	L232	L216
TM3	**3.43**	**I130**	**L142**	**L130**	–	TM6	6.40	I276	I296	I280
TM3	3.44	L131	V143	L131	–	TM5	**5.50**	**P217**	**P228**	**P212**
TM3	**3.46**	**M133**	**M145**	**M133**	–	TM6	**6.37**	**T273**	**T293**	**T277**
TM3	**3.47**	**T134**	**T146**	**S134**	–	TM5	5.58	I221	L232	L216
TM3	**3.47**	**T134**	**T146**	**S134**	–	TM5	**5.57**	**C224**	**C235**	**C219**
TM3	**3.47**	**T134**	**T146**	**S134**	–	TM5	**5.58**	**Q225**	**Y236**	**Y220**
TM3	**3.50**	**R137**	**R149**	**R137**	–	TM6	6.34	V270	V290	V274
TM4	**4.56**	**L170**	**L181**	**A167**	–	TM5	5.46	V213	I224	V208
TM4	**4.60**	**Q174**	**Q185**	**Q171**	–	TM5	5.38	Y205	Y216	Y200
TM5	5.47	F214	F225	Y209	–	TM6	6.52	F288	F308	F292
TM5	5.54	I221	L232	L216	–	TM6	6.40	I276	I296	I280
TM5	5.54	I221	L232	L216	–	TM6	6.41	V277	V297	V281
TM6	6.36	M272	M292	M276	–	TM7	7.57	S329	S352	T333
TM6	**6.47**	**C283**	**C303**	**C287**	–	TM7	7.42	A314	G337	A318
TM6	**6.50**	**P286**	**P306**	**P290**	–	TM7	7.38	L310	T333	V314
TM6	**6.51**	**F287**	**F307**	**F291**	–	TM7	7.38	L310	T333	V314

[a]Universal consensus numbering of GPCR Class A residues [30]

after molecular dynamics. In V2R and OTR, TM5 interactions with other helices are also weakened after MD, yet they remain stronger than in V1aR. It is worth noting strong interactions between TM3–TM5 and TM3–TM6 in the V2R complex and TM6–TM7 interactions involving conserved residues in the OTR complex. Interactions TM1–TM2 and TM1–TM7, as judged from Table 2, are weaker in V2R and OTR than in V1aR but still present. Interactions TM3–TM7 are weak as judged both by energy criteria (not shown) and distances (Table 2, absent), despite the fact that they have been reported as potentially relevant for receptor activation and signal transduction. [28] According to Table 2 and energy criteria (not shown), it seems that the most important interactions requisite for inactive V1aR are: TM1 L73–TM2 R91, TM1 V72–TM7 P345, TM2 L88–TM4 I171, TM3 R149–TM6 V290. A schematic summary of interhelical interactions is given in Fig. 1. Further examination of Table 2 and Fig. 1 indicates that the schemes of interhelical interactions in the three receptor–ligand complexes in the 1-ns timescale differ among each other, although there are many more similarities and overlaps

Table 3 Residues interacting with the ligand in the pairs of the V2R-**I**, V1aR-**I** and OTR-**I** complexes, after 1-ns MD relaxation. The residues unique only to V1aR are marked bold

TM1			TM2				TM3				TM6				TM7			
[a]	V2R	V1aR	OTR	[a]	V2R	V1aR	OTR	[a]	V2R	V1aR	OTR	[a]	V2R	V1aR	OTR	[a]	V2R	V1aR	OTR
				2.46		**L93**							I276			7.49	N321		
				2.50		**D97**		3.43	I130			6.44	Y280	Y300		7.45	N317		
																7.43	S315	S338	S319
				2.53		V100	V88					6.47		C303		7.42	A314	G337	A318
								3.39	S126			6.48		W304	W288	7.39	M311	A334	M315
				2.57	Q92	Q104										7.38		**T333**	
								3.36		M135	M123								
								3.35	G122	G134		6.51		F307	F291	7.36	V308	**T331**	
																7.35	F307	**I330**	F311
				2.61	Q96	Q108													
								3.32	Q119	Q131									
																7.32		**N327**	
1.35	E40	E54														7.31		**E326**	

[a] Universal consensus numbering of GPCR Class A residues [30]

Fig. 1 Scheme of interhelical interactions in the receptor–ligand complexes after MD. Connections among helices TM1–TM7 in rhodopsin via hydrogen bonds are given for [18]. Interactions loosened after MD are shown with *dotted lines*, while a TM5 motion observed during MD is indicated with *arrows*

between equivalent interactions in V1aR and OTR than in V1aR and V2R, which may be relevant with regard to a common signal transduction mechanism of V1aR and OTR involving activation of $G_{q/11}$, contrary to V2R, which activates G_s.

In Figs. 2, 3 and 4, features relevant to relaxed receptor–ligand structures (top) and their 1-ns MD trajectories (bottom) are shown. The bottom of Fig. 2 schematically illustrates the mobility of two lowest-energy V2R–**I** complexes. In both maps TM1–TM3, and TM8 (IL4) appear to be the most stable (or least mobile) helices during 1-ns MD. The remaining helices in both complexes are more mobile in the dynamics than the former ones. As expected, the relatively loose N- and C-termini and loops are the hottest receptor sites. Another common feature for both complexes are very (to 6–9 Å on average) and moderately (to 4–5.5 Å on average) mobile IL2 and EL1, respectively. Remaining sites of both receptors differ in mobility. In the left V2R–**I** complex still hot is IL1, in contrast to an unexpected quietness of the remaining loops and the N-terminus. On the other hand, in the right V2R–**I** complex, EL2, IL3 and EL3 undergo in the 1-ns MD quite large (to 4–8 Å on the average) motional drifts and, in addition, the central parts of TM5 and TM6 also exhibit a moderate (to 3–4 Å on average) move. In general, the loops and some helices in the right complex are more mobile than those in the left one on the 1-ns MD time scale. The fact that the *exo*-loops are most subject to these motions presumably indicates the nature of the motions related to a mutual adaptability and relaxation of the most sensitive sites of the receptor–ligand complex after initial docking. This is confirmed by a similar location (but a diverse orientation, see below) of both the relaxed V2R–**I** complexes, as can be seen in Fig. 2, top.

In the lower part of Fig. 3, similar contour maps are given for the two lowest-energy V1aR–**I** complexes.

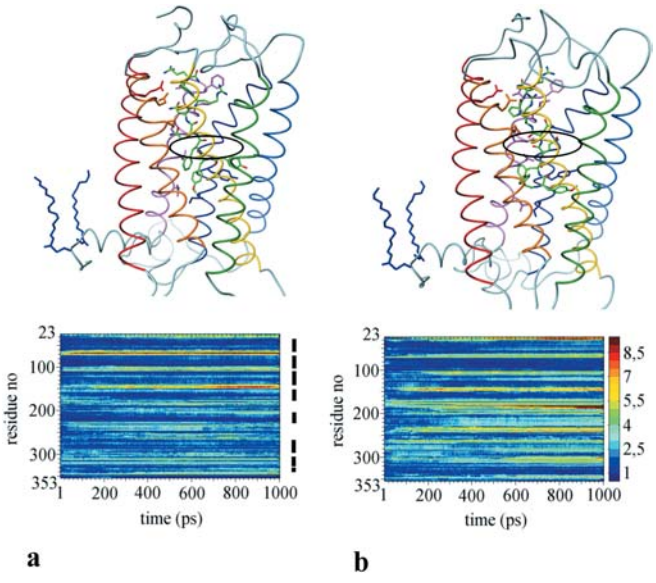

Fig. 2a–b Two best 1-ns MD-relaxed V2R–**I** complexes. *Top*: an overview of the relaxed structures. V2R is in the rope representation: TM1, *red*; TM2, *orange*; TM3, *yellow*; TM4, *green*; TM5, *bright blue*; TM6, *dark blue*; TM7, *violet*. Residues at contact distances, as defined in Table 2 with the ligand, are shown as sticks. The ligand is also in the stick representation, colored according to the atom types. The approximate space that would be occupied in RD by 11-*cis*-retinal is marked with an ellipse. *Bottom*: The plots illustrating a departure evolving in the MD (horizontal axis) of consecutive protein–ligand C^{α} atoms (vertical axis) from their starting position. The ligand is represented by the last eight sequence numbers. The contours are drawn every 0.5 Å, in agreement with the color scale defined on the far right. The TM helices are marked with vertical bars between both maps: TM1 35–64, TM2 74–102, TM3 110–142, TM4 153–176, TM5 203–228, TM6 269–296, TM7 305–327, TM8 330–340. For instance, the build-up of the green-to-orange band on the right map from ~540 to 1,000 ps involving residues ~295–305 corresponds to a gradual drift of EL3 away to average 4–7 Å from its starting position in the respective V2R–**I** complex

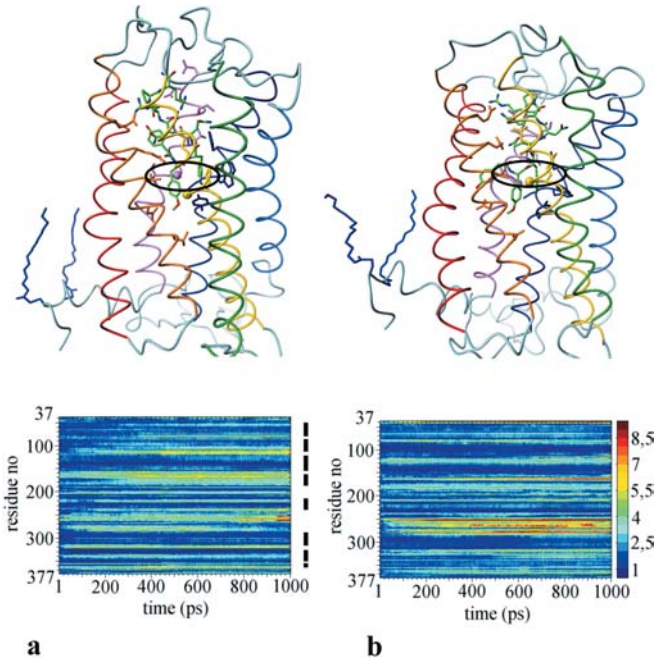

Fig. 3a–b Two best 1-ns MD-relaxed V1aR–**I** complexes. For details see legends to Fig. 2. TM1 49–78, TM2 86–114, TM3 122–154, TM4 164–187, TM5 214–239, TM6 289–316, TM7 328–350, TM8 354–364. Top: The interacting Gly residues, unique to this system, are marked as balls

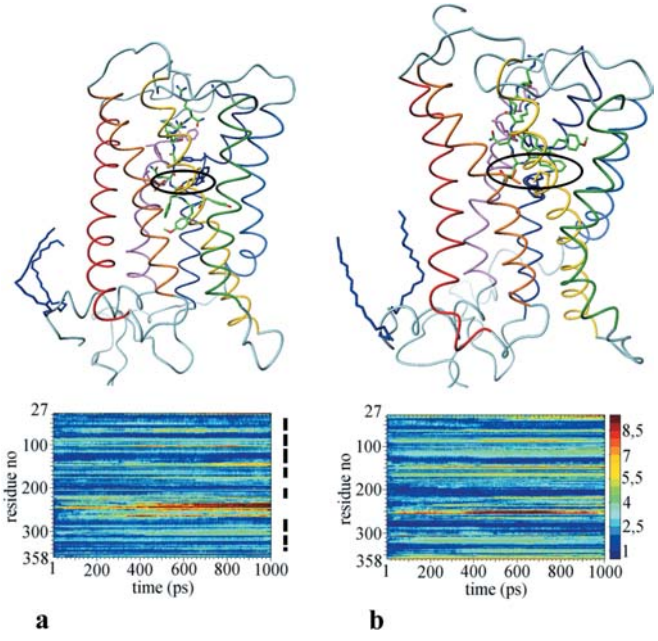

Fig. 4a–b Two best 1-ns MD-relaxed OTR–**I** complexes. For details see legends to Fig. 2. TM1 37–66, TM2 74–102, TM3 110–142, TM4 153–176, TM5 203–223, TM6 273–300, TM7 309–327, TM8 335–345

According to the maps both complexes exhibit a similar mobility, differently distributed on the structures of the two complexes only in modest details. Thus, the helices TM1–TM3 and TM6 are most stable in both complexes, IL2 and IL3 are most mobile (to 6–8 Å on average), in addition to a moderate (to 4.5–6 Å on average) mobility of EL1, EL3 and TM8(IL4) in the left complex, and a large mobility (to 8–9 Å on average) of the N-terminus in the right complex.

In the lower part of Fig. 4, analogical contour maps are given for the two lowest-energy OTR–**I** complexes. TM1, TM6 and EL2 uniformly appear relatively stable, while TM2 and both IL2 and IL3 uniformly appear to be moderately and highly, respectively, mobile in both OTR–**I** complexes. The remaining helices and loops demonstrate a modest mobility in both OTR–**I** complexes, except for the ligand, which in the right-hand complex exhibits a moderate to high mobility (to 5–7 Å on average).

On the whole, it is seen that the raw configurations of the lowest-energy complexes, directly after docking and

constrained simulated annealing, require diverse corrective relaxations, both within the same specific system, e.g. V2R–**I** complexes, and among the systems. The lowest-energy pairs of three receptor complexes exhibit a noticeable common behavior for the V1aR–**I** and OTR complexes only in the simulations, and even less common behavior among the three different receptor–ligand systems. We believe it would be premature to attribute any functional significance to these differences.

An outlook view of the complexes in the top Figs. 2 and 3 indicates that in relaxed receptor–**I** complexes the ligand typically assumes fairly extended conformations. In the V2R–**I** complexes, Fig. 2, the ligand in one complex faces the viewer with a side opposite to that in the other. This is not the case for the V1aR–**I** complexes, Fig. 3 top, in which the ligand is oriented in its pocket uniformly and similarly to the right-hand V2R–**I** complex, although it is significantly reconfigured. Both OTR–**I** complexes, in turn, are again different in the overview. While in the left one the ligand occupies its pocket in a manner somewhat similar to its left V2R–**I** counterpart, (compare Figs. 2 and 4 top left), in the other one it is more folded and placed shallower in the receptor than in any other complexes. In extension to the overviews in Figs. 2, 3 and 4 top, the details of the receptor–ligand interactions are given in Table 3.

Among the three receptors, the interacting set of amino acid residues is most extensive in V1aR, e.g. for TM2 five residues in V1aR versus two in V2R and one in OTR; for TM6 four residues in V1aR versus two in V2R and two in OTR; for TM7 eight residues in V1aR versus seven in V2R and four in OTR; see Table 3. Moreover, in TM3 and TM7, where comparable numbers of interactions (in V1aR versus V2R) are identified, they come from only partially overlapping regions in the respective TM helices, see Table 3 and Figs. 2, 3 and 4 top. Hence, these differences in TM2, TM6 and TM7 could possibly explain the selectivity of the **I** to V1aR against V2R and OTR. Interestingly, these data seem to be in general agreement with a study using a photoactivatable analog of the same linear V1aR antagonist. [29] The agreement especially concerns a seemingly prominent role of V1aR TM2 and TM7 in binding the ligands (e.g. compare Table 2 in [29] with Table 3 in this work).

In the centers of V1aR and V2R TM1 E1.35 (consensus notation [30]) and TM2 Q2.61 interact with R6 and R8 of the ligand, respectively. The most important interaction seems to be between TM2 Q108(2.61) from V1aR and ligands R6. This interaction is present in both relaxed V1aR complexes and in one V2R complex. There are two small cavities in the rhodopsin structure on its extracellular side [18] and a big one in the place occupied by11-*cis*-retinal in the dark rhodopsin. [4] In the equivalent place of V1aR, see Fig. 3, we observe a strong hydrophobic interaction between TM6 Y300(6.44) and W304(6.48) with the OH–Phaa group. These interactions are also present in V2R and OTR, involving only Y280(6.44) and W288(6.48), respectively, but not both residues, contrary to V1aR. Furthermore, only in V1aR the ligand almost ideally fits this place, thus providing another argument for 4-OH-phenylacetyl-*D*-Y(Me)FQN-RPR-NH_2 selectivity to V1aR.

The results obtained are preliminary and the suggested interactions should be considered only as starting hypotheses for the experimental studies, which would confirm or disprove them. Given that many aspects of mechanisms of GPCR action are still unsolved, the results of the docking simulations may be considered as tips for experimental research, especially in site-directed mutagenesis analysis and the search for amino acid residues responsible for drugs activities.

References

1. (a) Bankir L (2001) Cardiovasc Res 51:372–390; (b) Birnbaumer M (2001) Cardiovasc Res 51:409–415; (c) Wong LL, Verbalis JG (2001) Cardiovasc Res 51:391–402
2. Thibonnier M, Berti-Mattera LN, Dulin N, Conarty DM, Mattera R (1998) In: Urban IJA, Burbach JPH, DeWied D (eds) Advances in brain vasopressin. Elsevier, Amsterdam, pp 143–158
3. Gimpl G, Fahrenholz F (2001) Physiol Rev 81:629–683
4. Palczewski K, Kumasaka T, Hori T, Behnke CA, Motoshima H, Fox BA, Le Trong I, Teller DC, Okada T, Stenkamp RE, Yamamoto M, Miyamoto M (2000) Science 289:739–745
5. Ballesteros J, Palczewski K (2002) Curr Opinion Drug Discovery Develop 4:561–574
6. Sugimoto T, Saito M, Mochizuki S, Watanabe Y, Hashimoto S, Kawashima H (1994) J Biol Chem 269:27088–27092
7. de Keyzer Y, Auzan C, Lenne F, Beldjord C, Thibonnier M, Bertagna X, Clauser E (1994) FEBS Lett 356:215–220
8. Laszlo FA, Laszlo Jr F, de Wied D (1991) Pharmacol Rev 43:73–108
9. Liu J, Wess J (1996) J Biol Chem 271:8772–8778
10. Chini B, Mouillac B, Ala Y, Balestre MN, Trumpp-Kallmeyer S, Hoflack J, Elands J, Hibert M, Manning M, Jard S, Barberis C (1995) EMBO J 14:2176–2182
11. Ufer E, Postina R, Gorbulev V, Fahrenholz F (1995) FEBS Lett 362:19–23
12. Barberis C, Balestre MN, Jard SD, Tribollet E, Arsenijevic Y, Dreifuss JJ, Bankowski K, Manning M, Chan WY, Schlosser SS, Holsboer F, Ellands J (1995) Neuroendocrinology 62:135–148
13. Forster MJ (2002) Micron 33:365–384
14. Thompson JD, Gibson TJ, Plewniak F, Jeanmougin F, Higgins DG (1997) Nucleic Acids Res 24:4876–4882
15. Corpet F (1988) Nucleid Acids Res 16:10881–10890
16. SYBYL 6.6 (1999) Tripos Inc, 1699 South Hanley Rd, St Louis, MO 63144, USA
17. Liebmann C, Böhmer FD (2000) Curr Med Chem 7:911–943
18. Teller DC, Okada T, Behnke CA, Palczewski K, Stenkamp RE (2001) Biochemistry 40:7761–7772
19. Schmidt MW, Baldridge KK, Boatz JA, Elbert ST, Gordon MS, Jensen JJ, Koseki S, Matsunaga N, Nguyen KA, Su S, Dupuis M, Montgomery JA (1993) J Comput Chem 14:1347–1363
20. Bayly CI, Cieplak P, Cornell WD, Kollman P (1993) J Phys Chem 97:10269–10280
21. Perlman DA, Case DA, Caldwell JW, Cheatham III TE, Ross WS, Simmerling C, Darden T, Merz KM, Stanton RV, Radmer R, Seibel GL, Singh UC, Weiner P, Kollman PA (1997) AMBER 5.0. University of California, San Francisco
22. Czaplewski C (1998) Thesis. Faculty of Chemistry, University of Gdańsk
23. Czaplewski C, Pasenkiewicz-Gierula M, Ciarkowski J (1999) Int J Quantum Chem 73:61–70

24. Cambridge Structural Database System (2001) Cambridge Crystallographic Data Centre, Cambridge, UK
25. Morris GM, Goodsell DS, Halliday RS, Huey R, Hart WE, Belew RK, Olson AJ (1998) J Comput Chem 19:1639–1662
26. Kirkpatrick S, Gelate Jr CD, Vecchi MP (1983) Science 220:671–680
27. Murzyn K, Róg T, Jezierski G, Takaoka Y, Pasenkiewicz-Gierula M (2001) Biophys J 81:170–183
28. Ulloa-Aguirre A, Stanislaus D, Janovick JA, Conn PM (1999) Arch Med Res 30:420–435
29. Phalipou S, Seyer R, Cotte N, Breton C, Barberis C, Hibert M, Mouillac B (1999) J Biol Chem 274:23316–23327
30. Ballesteros JA, Weinstein H (1995) Methods Neurosci 25:366–425